Asian Journal of Chemistry; Vol. 37, No. 9 (2025), 2135-2140
ASIAN JOURNAL OF CHEMISTRY
https://doi.org/10.14233/ajchem.2025.34148

Enhancing Optical and Antioxidant Functionality in Zinc Doped Nickel Sulfide Nanoparticles

C. SELVAKUMAR[1,*], V.T. GEETHA[1], A. JAYANTHI[2] and D.V. SRIDEVI[3]

[1]Department of Chemistry, Sri Sairam Engineering College, Tambaram, Chennai-600044, India
[2]Department of Chemistry, Panimalar Engineering College, Chennai-600123, India
[3]Department of Chemistry, Rajalakshmi Institute of Technology, Kuthambakkam, Thiruvallur-600124, India

*Corresponding author: E-mail: selvakumar.chem@sairam.edu.in

Received: 29 May 2025 *Accepted*: 11 July 2025 *Published online*: 30 August 2025 AJC-22092

This study focuses on the optical and antioxidant properties of zinc-doped nickel sulfide (Zn–NiS) nanoparticles synthesized *via* an eco-friendly co-precipitation method, using varying zinc concentrations of 10%, 20% and 30%. In structural analyses using IR, SEM, TEM, and XRD techniques, Zn-NiS nanoparticles exhibited distinct features compared to undoped nickel sulfide (NiS), with EDAX confirming its crystalline organization. At higher Zn doping levels, optical studies based on Tauc equation revealed a redshift in the absorption edge and a reduction in band gap energy, attributed to defect-induced modifications in the electronic structure. Structural and morphological investigations confirmed phase stability (hexagonal) and demonstrated doping-dependent morphological transitions—from rod-like structures to porous clusters. Notably, 30% Zn-doped NiS exhibited approximately 95% inhibition at a concentration of 1000 µg/mL in DPPH radical scavenging assays, highlighting its remarkable antioxidant activity. These findings underscore the dual functional potential of Zn-NiS for sustainable technological applications, particularly in the biomedical field (as antioxidants) and in optoelectronics (*via* tunable band gaps).

Keywords: Zinc-doped nickel sulfide nanoparticles, Optical band gap modulation, Antioxidant activity, DPPH radical scavenging.

INTRODUCTION

The global shift toward eco-friendly synthesis aims to reduce environmental hazardousness and reliance on the fossil fuels. Photovoltaic solar cells, which convert sunlight into electricity, are central to renewable energy. However, traditional silicon-based cells face challenges like limited light absorption and efficiency losses at high temperatures [1]. Semiconductor nanomaterials, particularly doped nanoparticles, offer promising solutions [2]. Among them, zinc-doped nickel sulfide (Zn-doped NiS) nanoparticles stand out for their tunable optical and electrical properties, making them ideal for next-generation solar energy applications [3].

The efficiency of solar cells is heavily influenced by the band gap of semiconductor, which determines the energy required to excite electrons from the valence to conduction band. Silicon (~1.1 eV) primarily absorbs visible light, leaving substantial portions of the solar spectrum namely ultraviolet and infrared underutilized. To address this, researchers are developing nanomaterials with customizable band gaps to broaden absorption and reduce energy loss. Doping transition metal sulfides like NiS with zinc introduces defect states and adjusts electronic structures, enabling red-shifted absorption and enhanced charge separation [4].

In addition to their potential in energy conversion, Zn-doped metal oxide/sulfide nanoparticles might demonstrate promising antioxidant properties [5-7]. The incorporation of zinc ions into the sulfide matrix enhances surface reactivity, which facilitates the neutralization of free radicals. A widely employed method for evaluating antioxidant capacity is the 1,1-diphenyl-2-picrylhydrazyl (DPPH) assay, which relies on the ability of electron-donating agents to reduce DPPH radicals. Owing to their redox active surfaces, Zn-doped NiS nanoparticles exhibit a concentration-dependent inhibition of DPPH radicals, comparable to the activity of standard antioxidants such as ascorbic acid. In this study, the synthesis, physico-chemical characterization and dual-functional properties of Zn-doped NiS nanoparticles are systematically explored.

EXPERIMENTAL

All chemicals used in the synthesis were of analytical grade and used without further purification. Nickel(II) chloride hexahydrate ($NiCl_2·6H_2O$) was used as nickel precursor (Loba Chemie, India), zinc chloride ($ZnCl_2$) served as dopant source (Merck, India) and sodium sulfide nonahydrate ($Na_2S·9H_2O$) acted as the sulfur source (SRL, India). Polyvinyl alcohol (PVA, M.W. ~30,000–70,000) was employed as a capping and stabilizing agent (HiMedia), while methanol (SD Fine Chemicals, India) and deionized water were used as solvents throughout the process.

Fourier transform infrared spectroscopy (FTIR) was performed on a Perkin-Elmer Spectrum 2 spectrometer in the range of 4000–400 cm^{-1} using the KBr pellet method. The crystalline structure was analyzed using X-ray diffraction (XRD) with a PANalytical X′Pert PRO diffractometer equipped with Cu*K*α radiation (λ = 1.5406 Å) over a 2θ range of 10–80º. Surface morphology was examined using a JEOL JSM-6390LV Scanning Electron Microscope (SEM) and the internal structure and crystallinity were studied using a JEOL JEM-2100 transmission electron microscope (TEM) operating at 200 kV along with Selected Area Electron Diffraction (SAED) patterns. Optical absorption properties were assessed using a JASCO V-730 UV-Visible spectrophotometer in the 200–800 nm range.

Preparation of zinc doped nickel sulfide nanoparticles with various compositions: Various compositions of nickel chloride and zinc chloride were dissolved in a 100 mL of aqueous methanol (1:1) under constant magnetic stirring. A fixed amount of $Na_2S·9H_2O$ dissolved in 50 mL deionized water, was then added dropwise to the solution. This was followed by the addition of another 50 mL of methanol containing 0.5 g of PVA as a stabilizing agent. The reaction mixture was stirred continuously for approximately 30 min, leading to the formation of a fine precipitate of Zn–NiS nanoparticles. The resulting precipitate was collected by vacuum filtration, washed thoroughly with methanol and dried using a microwave oven. A fine yellow powder was obtained, indicating the successful formation of Zn–NiS nanocomposites. Samples with varying doping concentrations (10%, 20% and 30%) were synthesized by varying the molecular mass ratio of zinc and nickel precursors as detailed in Table-1.

TABLE-1

Zn doping (%)	$NiCl_2·6H_2O$ (mmol)	$ZnCl_2$ (mmol)	$Na_2S·9H_2O$ (mmol)
0% (undoped)	1.0	0.0	1.0
10	0.9	0.1	1.0
20	0.8	0.2	1.0
30	0.7	0.3	1.0

Antioxidant activity: A methanolic solution of 1,1-diphenyl-2-picrylhydrazyl (DPPH) was prepared at a concentration of 0.135 mM to evaluate the antioxidant activity of Zn-doped NiS nanoparticles. For the assay, 180 µL of the DPPH solution was mixed with 20 µL of Zn-doped NiS nanoparticles suspensions at varying concentrations. To prepare the test samples, 5 mg of Zn-doped NiS nanoparticles were dispersed in 1 mL of HPLC grade water to yield a stock solution. Working solutions at concentrations of 10, 50, 100, 500 and 1000 µg/mL were prepared by serial dilution in HPLC water, followed by sonication for 10 min to ensure uniform dispersion. After mixing with DPPH, the reaction mixtures were incubated in the dark at room temperature for 30 min and then measured at 517 nm using a BioTek ELx800 microplate reader. Methanol served as the blank, and ascorbic acid was used as a positive control. All measurements were performed in triplicate and the percentage of DPPH radical scavenging was calculated to assess the antioxidant activity. The experiments were performed in triplicate and percentage scavenging activity was calculated using following equation:

$$\text{Scavenging activity (\%)} = \frac{\text{Abs}_{\text{control}} - \text{Abs}_{\text{sample}}}{\text{Abs}_{\text{control}}} \times 100$$

All the experiments were conducted in triplicate and means with standard deviation were calculated [8]. The antioxidant activity of synthesized zinc doped nickel sulfide nanoparticles was evaluated by DPPH radical scavenging assay.

RESULTS AND DISCUSSION

FTIR spectral studies: The structural changes induced by doping were investigated using FTIR spectroscopy, as illustrated in Fig. 1. The incorporation of zinc into NiS significantly alters its physico-chemical properties compared to the undoped material. FTIR spectra of Zn-doped NiS nanoparticles with doping concentrations of 10%, 20% and 30% exhibit distinct vibrational features indicative of compositional modifications. A broad absorption band observed around 3400 cm^{-1} corresponds to O–H stretching vibrations, likely arising from adsorbed moisture or surface hydroxyl groups. The gradual decrease in the intensity of this band with increasing Zn content suggests reduced surface hydroxylation due to doping. Additionally, the absorption band near 1630 cm^{-1} is attributed to H–O–H bending vibrations of molecular water, with similar doping-dependent variations in intensity. In the fingerprint region (600-400 cm^{-1}), prominent peaks between 620–680 cm^{-1} are assigned to Ni–S stretching vibrations, confirming the formation of the NiS phase. The

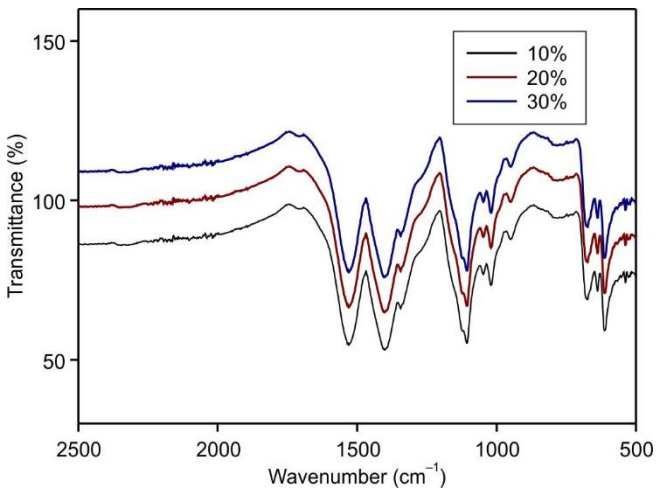

Fig. 1. FTIR interpretation for Zn:Ni S nanoparticle

substitution of Zn^{2+} for Ni^{2+} in the NiS lattice induces localized structural distortions, leading to modifications in the metal-sulfur bonding environment. These changes are reflected in the shifts, intensity variations, and sharpening of vibrational peaks with increasing Zn doping levels [9,10]. The observed spectral variations confirm the successful incorporation of Zn into the NiS matrix and provide insights into the altered local bonding structure, which may significantly influence the material's physical and chemical behaviour [11].

XRD studies: The XRD patterns (Fig. 2) suggest that the interaction between Zn and NiS involves not only surface adsorption but also covalent bonding, indicating effective incorporation of Zn into the NiS lattice [12,13]. The observed diffraction peaks at 2θ values of approximately 8º, 12º and 18º correspond to the crystalline planes of the doped NiS phase. Based on the full width at half maximum (FWHM) of these peaks, the average crystallite sizes were estimated using the Scherrer equation to be approximately 2 nm, 3 nm and 4.5 nm, respectively. These results confirm the crystalline nature of the nanoparticles and suggest a regular arrangement within the crystal lattice [14]. Well-defined diffraction peaks corresponding to the hexagonal phase of NiS are clearly observed for samples doped with 10%, 20%, and 30% Zn. This indicates that the fundamental crystal structure remains intact upon doping. The sharp and intense peaks are indicative of high crystallinity in the synthesized materials [15]. Significantly, the positions of the major peaks remain largely unchanged with increasing Zn content, implying successful substitution of Zn^{2+} ions into the NiS lattice without disrupting the overall crystal symmetry. Minor variations in the peak width and intensity were observed; however, a general increase in peak intensity with higher Zn doping levels may suggest improved crystallite growth and lattice ordering. The absence of secondary phases further confirms the phase purity and effective doping of Zn into the NiS matrix.

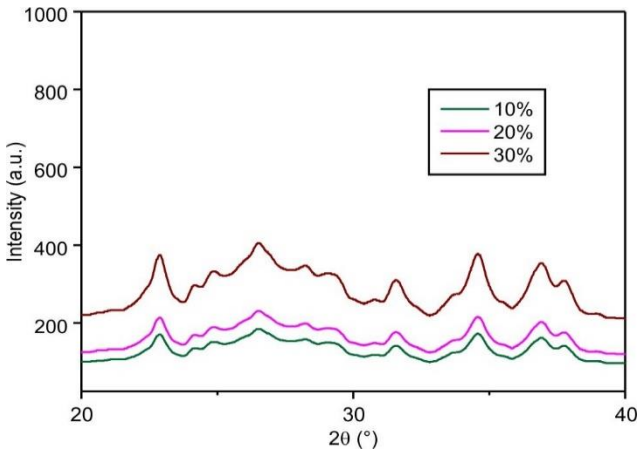

Fig. 2. XRD interpretation for Zn:Ni S nanoparticle

SEM studies: The surface morphology and structural features of Zn-doped NiS nanoparticles were examined using scanning electron microscopy (SEM), as shown in Fig. 3 for samples I, II and III. These images reveal that the nanoparticles exhibit predominantly globular shapes with varying particle sizes. The SEM examination of the 10%, 20% and 30% Zn-doped NiS samples reveals significant morphological evolution with increasing Zn content. SEM analysis confirms a relatively uniform distribution of particles across the examined regions [7], indicating effective dispersion and homogeneity. At 10% doping, the nanoparticles display rod-like or needle-shaped structures, suggestive of anisotropic growth and a high degree of crystallinity [16]. With 20% Zn doping, the morphology shifts to a granular form comprising densely packed, nearly spherical particles, indicating suppression of directional growth. At 30% Zn concentration, the particles form a sponge-like porous network characterized by increased surface roughness and higher levels of agglomeration. These progressive changes in microstructure imply that Zn^{2+} ions substantially affect the nucleation and growth processes during synthesis, thereby influencing the final morphology and surface properties of the nanoparticles.

TEM and SEAD studies: Transmission electron microscopy (TEM) images of Zn-doped NiS nanoparticles, presented in Fig. 4, reveals a network of interconnected quasi-spherical particles forming an aggregated and porous architecture. At higher magnifications, individual nanoparticles become more distinguishable and the variation in contrast across regions suggests the coexistence of well-defined crystalline domains within a more disordered matrix. The observed particle sizes are generally below 50 nm, making them highly suitable for applications that benefit from a high surface-to-volume ratio. The selected area electron diffraction (SAED) pattern further confirms the polycrystalline nature of the material, displaying distinct concentric rings correspond-

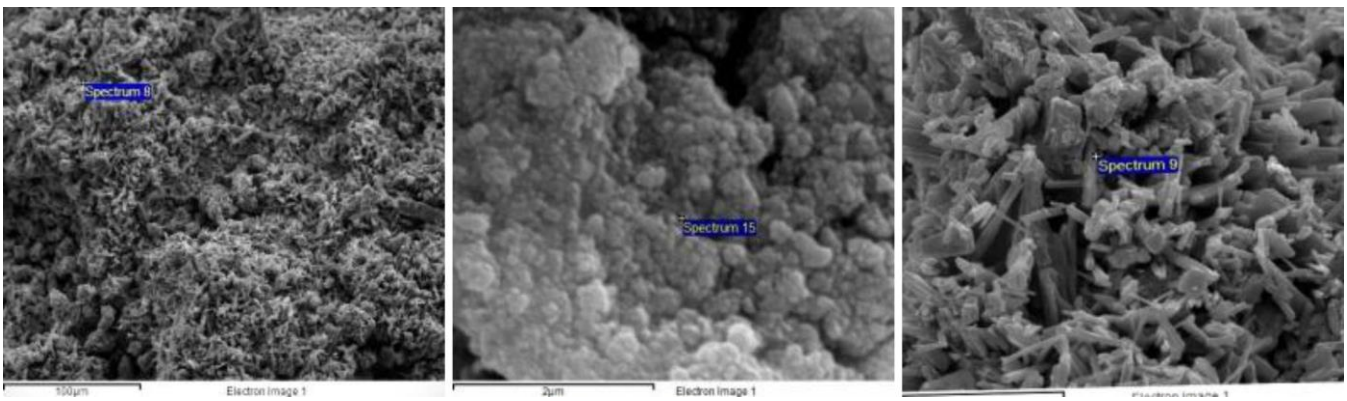

Fig. 3. SEM images of Zn:NiS nanoparticles

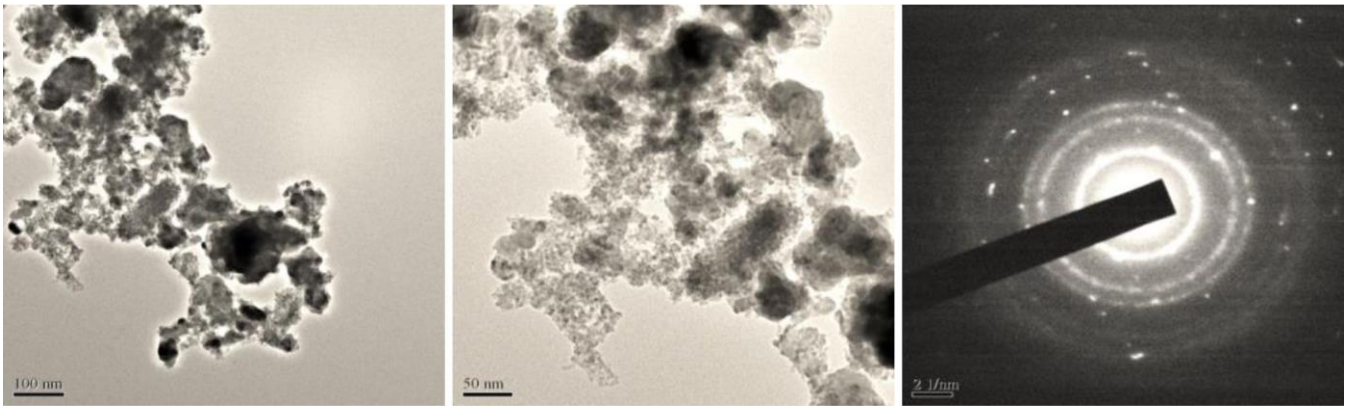

Fig. 4. TEM and SEAD pattern of zinc doped nickel sulfide nanoparticles

ding to specific crystallographic planes [17,18]. These rings are indicative of high crystallinity and phase purity. Notably, Zn doping does not disrupt the overall integrity of the NiS crystal lattice but may induce slight variations in interplanar spacing due to the substitution of Ni^{2+} by Zn^{2+} ions. Such structural modifications can enhance the functional performance of the material, supporting its potential use in applications such as energy storage devices, chemical sensors, and heterogeneous catalysis.

UV-Visible studies: The UV–visible absorption spectra of Zn-doped NiS nanoparticles, shown in Fig. 5, reveal significant changes in optical behaviour with increasing Zn concentrations (10%, 20% and 30%). The 30% Zn-doped sample demonstrates the highest absorbance intensity, indicating enhanced light-harvesting efficiency, which is favourable for the optoelectronic and photocatalytic applications [19]. A progressive increase in absorption across the series confirms the role of Zn incorporation in modifying the optical density of the material. Moreover, a redshift in the absorption edge is observed with higher Zn content, suggesting a reduction in band gap energy. This shift is attributed to increased electron density and lattice strain arising from Zn^{2+} substitution, which alters the band structure and dielectric properties of the material. The absence of sharp excitonic features in the spectra implies that doping effects dominate over quantum confinement, indicating that the observed changes are primarily structural and electronic rather than size-related. These observations are consistent with prior studies on transition-metal-doped semiconductor systems, where controlled doping effectively tunes the band gap and improves the optical performance [20,21]. Overall, Zn doping emerges as an efficient strategy to tailor the optical characteristics of NiS nanoparticles for energy-oriented applications. The estimated optical band gap of approximately 5.25 eV, illustrated in Fig. 6, is significantly larger than those of typical semi-conductors (< 3.5 eV), aligning more closely with wide band gap insulators. However, this apparent value is modulated by localized defect states or intermediate energy levels introduced through Zn^{2+} substitution. These defect states enable sub-band-gap transitions, thereby extending absorption into the visible region. Furthermore, the structural distortion and altered electronic density due to Zn doping influence the material's dielectric response, potentially enhancing its suitability for high-capacitance devices and catalytic systems [22]. While

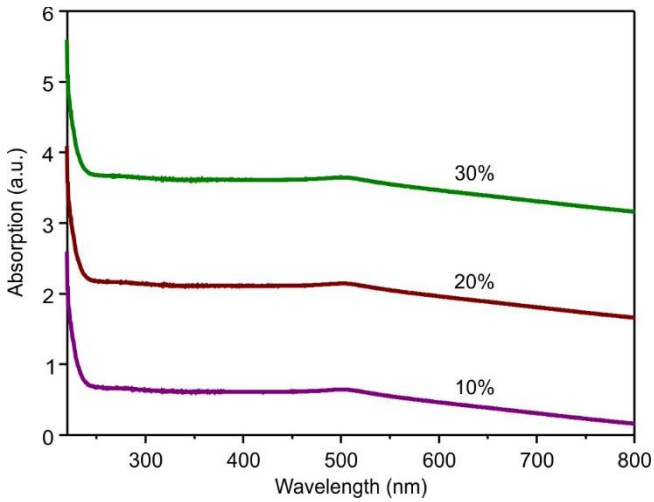

Fig. 5. UV-Visible spectrum of zinc doped nickel sulfide

quantum confinement effects are minimal in this context, doping-induced compositional and structural changes clearly dominate the optical response, underscoring the tunability and functional versatility of Zn-doped NiS nanoparticles.

Antioxidant activity: The antioxidant activity of Zn:NiS nanoparticles was evaluated using the DPPH radical scavenging assay, with ascorbic acid serving as the reference standard. Both Zn:NiS and ascorbic acid exhibited a concentration-dependent increase in radical scavenging efficiency across the tested concentration range (10–1000 μg/mL). Significantly, Zn:NiS nanoparticles consistently outperformed the standard at all concentrations. At the highest tested dose (1000 μg/mL), Zn:NiS achieved a scavenging efficiency of 94.71%, nearly double that of ascorbic acid, which demonstrated 50.54% inhibition. Even at the lowest concentration (10 μg/mL), Zn:NiS exhibited 5.65% inhibition, compared to 3.46% by the standard. These results (Table-2), underscore the superior antioxidant potential of Zn doped NiS nanoparticles [23]. The enhanced scavenging behaviour is attributed to the synergistic effects introduced by Zn doping within the NiS matrix. Zinc incorporation alters the electronic structure and introduces lattice defects, creating localized energy states that facilitate improved electron transfer to DPPH radicals. Furthermore, the redox-active Ni^{2+}/Ni^{3+} couples inherent to the NiS lattice contribute to effective radical neutralization by promoting electron transport and stabilizing reactive

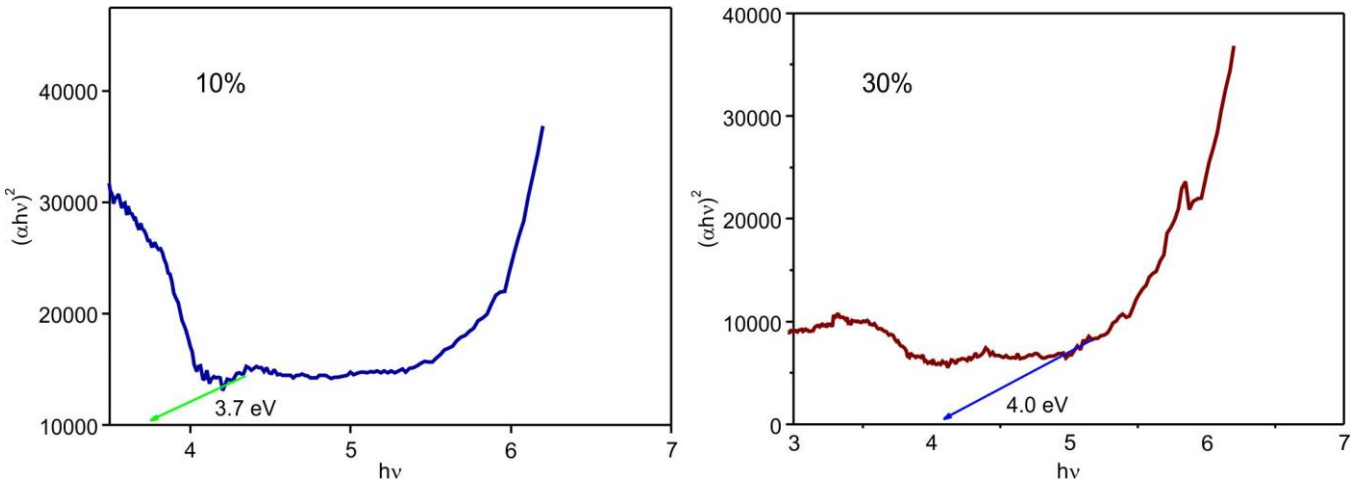

Fig. 6. Optical band graph of zinc doped nickel sulfide

TABLE-3
COMPARATIVE STUDY WITH VARIOUS NANOMATERIALS

Metal sulfide	Synthesis method	Morphology	Max. DPPH scavenging activity (%)	Ref.
Zn-doped NiS	Co-precipitation (green method with PVA)	Porous clusters at 30% doping	94.71	Present study
CuS nanoparticles	Hydrothermal	Nanospheres	~82.00	[22]
Co-doped MoS_2	Solvothermal	Nanosheets	~88.00	[26]
Mn-doped FeS_2	Chemical co-precipitation	Granular morphology	~90.00	[9]
Ni-doped SnS_2	Microwave-assisted hydrothermal	Nanoplates	~85.00	[23]

TABLE-2
ANTIOXIDANT ANALYSIS OF ZINC DOPED NICKEL SULFIDE

Conc. (µg)	Ascorbic acid (standard)		Zn:NiS	
	Absorbance	Inhibition (%)	Absorbance	Inhibition (%)
10	1.058	3.46	1.034	5.65
50	0.954	12.96	0.642	41.42
100	0.723	34.03	0.209	80.93
500	0.618	43.62	0.067	93.88
1000	0.542	50.54	0.058	94.71

species through reduction mechanisms [24,25]. The observed dose-dependent activity and structural robustness suggest that tuning Zn doping levels between 10% and 30% can effectively modulate redox behaviour and surface reactivity. These findings point to the potential of Zn doped NiS nanoparticles as high-performance antioxidant materials. Moreover, Table-3 emphasizes that Zn-doped NiS nanomaterial shows superior antioxidant activity (94.71%) compared to other reported metal sulfide systems synthesized by different methods.

Conclusion

Zinc-doped nickel sulfide (Zn-NiS) nanoparticles with varying Zn concentrations (10%, 20% and 30%) were successfully synthesized and their structural, morphological, optical, and antioxidant properties were systematically investigated. The XRD and FTIR analyses confirmed the retention of the hexagonal NiS phase upon Zn incorporation, while also indicating structural modifications and reduced surface hydroxylation at higher doping levels. Morphological characterization using SEM and TEM techniques revealed a progressive transformation from rod-like structures to porous, interconnected aggregates with increasing Zn content. The polycrystalline nature of the doped nanoparticles was further validated by SAED patterns. The optical studies demonstrated a redshift in the absorption edges and a reduction in band gap energy to approximately 5.25 eV, attributed to Zn-induced alterations in the electronic structure and lattice strain. Antioxidant performance assessed using the DPPH radical scavenging assay showed a significant concentration-dependent response, with Zn-NiS nanoparticles achieving up to 94.71% inhibition at 1000 µg/mL, surpassing the standard antioxidant, ascorbic acid. This enhanced activity is associated with the synergistic effects of Zn doping, including surface defect formation, increased porosity and the presence of redox-active Ni^{2+}/Ni^{3+} couples.

CONFLICT OF INTEREST

The authors declare that there is no conflict of interests regarding the publication of this article.

REFERENCES

1. K. ElKhamisy, H. Abdelhamid, E.M. El-Rabaie and N. Abdel-Salam, *Plasmonics*, **19**, 1 (2024); https://doi.org/10.1007/s11468-023-01905-x
2. X. Wang, Y. Li, B. Zhang and G. Sun, *J. Mater. Chem. A*, **3**, 18922 (2015); https://doi.org/10.1039/C5TA04346C
3. S. Kumar, A. Sharma and R. Mehta, *ACS Appl. Nano Mater.*, **6**, 6543 (2023); https://doi.org/10.1021/acsanm.3c00471

4. J. Younus, W. Shahzad, B. Ismail, T. Fazal, M. Shah, S. Iqbal, A.H. Jawhari, N.S. Awwad and H.A. Ibrahium, *RSC Adv.*, **13**, 27415 (2023); https://doi.org/10.1039/D3RA04011A
5. K. Patel, H. Joshi and A. Singh, *Appl. Sci.*, **13**, 12456 (2023); https://doi.org/10.3390/app132212456
6. A. Batool, A. Azizullah, K. Ullah, S. Shad, F.U. Khan, M.F. Seleiman, T. Aziz and U. Zeb, *BMC Plant Biol.*, **24**, 820 (2024); https://doi.org/10.1186/s12870-024-05525-3
7. C. Selvakumar and M. Deepa, *Indian J. Chem. Technol.*, **27**, 9 (2020).
8. A. Yadav, P. Sharma and R. Singh, *Polym. Rev.*, **62**, 765 (2022); https://doi.org/10.1080/15583724.2021.2014517
9. L. Wang, H. Zhou and Y. Li, *Nanoscale Adv.*, **5**, 789 (2023); https://doi.org/10.1039/D2NA00834F
10. C. Selvakumar, V.T. Geetha, S. Sathiyamoorthi and R. Sharan, *J. Nonlinear Opt. Phys. Mater.*, **34**, 2450037 (2025); https://doi.org/10.1142/S0218863524500371
11. J. Gong, X. Wang, H. W, X. Dong, J. Li, F. Yang, A. Yuan and H. Ji, *Appl. Surf. Sci.*, **605**, 154702 (2022); https://doi.org/10.1016/j.apsusc.2022.154702
12. L. Kumaresan, C. Selvakumar, G. Shanmugavelayutham and K. Jayasankar, *New J. Chem.*, **47**, 17080 (2023); https://doi.org/10.1039/D3NJ02526H
13. H. Ali, N. Ahmed and S. Khan, *Environ. Sci. Nano*, **10**, 1123 (2023); https://doi.org/10.1039/D2EN01122A
14. Y. Xue, J. Xiao, K. Li, H. Gu, Q. Lu and Y. Pang, *J. Nanopart. Res.*, **23**, 265 (2021); https://doi.org/10.1007/s11051-021-05379-y
15. C. Selvakumar and M. Deepa, *Int. J. Chemtech Res.*, **7**, 2675 (2010).
16. Q. Li, Z. Feng and Y. Liu, *Adv. Energy Mater.*, **12**, 2201234 (2022); https://doi.org/10.1002/aenm.202201234
17. M. Avateffazeli, S.I. Shakil, H. Pirgazi, B. Shalchi-Amirkhiz, M. Mohammadi and M. Haghshenas, *Mater. Today Commun.*, **36**, 106581 (2023); https://doi.org/10.1016/j.mtcomm.2023.106581
18. M. Kasaeian-Naeini, M. Sedighi, R. Hashemi and H. Delavar, *Ceram. Int.*, **49**, 16981 (2023); https://doi.org/10.1016/j.ceramint.2023.02.069
19. J. Lee, *Vib. Spectrosc.*, **123**, 103456 (2022); https://doi.org/10.1016/j.vibspec.2022.103456
20. I. Arnay, A. Serrano, V. Braza, R. Cid, A.M. Sánchez, J. López-Sánchez, G.R. Castro and J. Rubio-Zuazo, *J. Alloys Compd.*, **947**, 169540 (2023); https://doi.org/10.1016/j.jallcom.2023.169540
21. V. Blanchet, D. Descamps, S. Petit, Y. Mairesse, B. Pons and B. Fabre, *Phys. Chem. Chem. Phys.*, **23**, 25612 (2021); https://doi.org/10.1039/D1CP03569J
22. Y. Fang, L. Zhang and J. Liu, *Biomater. Sci.*, **11**, 1532 (2023); https://doi.org/10.1039/D2BM01987C
23. V. Tiwari, S. Gupta and M. Kumar, *Free Radic. Res.*, **57**, 245 (2023); https://doi.org/10.1080/10715762.2023.2194428
24. H. Lu, Q. Wang, J. Chen, H. Zhang, J. Ding, Y. Nuli, J. Yang and J. Wang, *Energy Storage Mater.*, **63**, 102944 (2023); https://doi.org/10.1016/j.ensm.2023.102994
25. L. Wagner, B. Kenzhebayeva, B. Dhaini, S. Boukhlef, A. Moussaron, S. Mordon, C. Frochot, C. Collet and S. Acherar, *Coord. Chem. Rev.*, **470**, 214702 (2022); https://doi.org/10.1016/j.ccr.2022.214702
26. Y. Zhang, L. Liu and M. Chen, *J. Mater. Chem. B Mater. Biol. Med.*, **10**, 1892 (2022); https://doi.org/10.1039/D1TB02563E